Shahid *Boundary Value Problems* (2018) 2018:84
https://doi.org/10.1186/s13661-018-1001-3

Boundary Value Problems
a SpringerOpen Journal

RESEARCH Open Access

Role of a structural parameter in modelling blood flow through a tapering channel

N. Shahid[1,2*]

*Correspondence:
nash_shhd@hotmail.com;
nazishshahid@fccollege.edu.pk;
nshahid@princeton.edu
[1]Department of Mathematics, Forman Christian College, A Chartered University, Lahore, Pakistan
[2]Department of Mechanical and Aerospace Engineering, Princeton University, Princeton, USA

Abstract

An investigation of thixotropic parameter influence on blood flow in a stenosed tapered vessel has been carried out by means of analytical and numerical methods. We have studied how variation of a parameter in a range [0, 1], chosen following the evolution of transient shear, flows with time in this particular range and impacts the dynamics of an unsteady, non-Newtonian fluid flow. An approximation of a simpler dynamical system was approached with the help of a particular set of non-dimensional variables. Unique representations of axial velocity, shear stress and flow rate have been made such that their dependence on pressure gradient can be further analysed. Some factors that either impede the flow or help to accelerate it in a narrow channel in addition to varying yield stress and thixotropic parameter have been numerically investigated. The purpose of the current investigation is also to decide whether the particular model parameter regulates the dynamics of flow in a vessel differently from other known non-Newtonian models and what specific range or values of this parameter bring this model's results to coincide with other models' results

Keywords: Thixotropy; Blood flow; Tapering; Axial velocity; Pressure-gradient; Structural parameter

1 Introduction

The understanding of vascular dynamics and mechanism of arterial blood rheology has been important not only for advancement of medical science but also to overcome the development of complexities caused by overlooking minute details that can potentially change the course of a system. The arterial malfunction and disturbance in blood flow propagation caused by stenosis have been a subject of long-term investigation and has added to valuable material to smooth understanding and better projection of rather a complex scenario. The study of modelling of blood flow through arterial stenosis by means of theoretical and experimental methods has been done to establish grounds for implanted vascular system.

Over the course of time, many researchers have contributed to this area of investigation. Young [1] and Young and Tsai [2] laid grounds for the study of dynamics of flow through stenosed arteries and recorded results for steady flow on the matter. An investigation of flow dynamics in a tubular channel on arterial stenosis with inclusion of time

© The Author(s) 2018. This article is distributed under the terms of the Creative Commons Attribution 4.0 International License (http://creativecommons.org/licenses/by/4.0/), which permits unrestricted use, distribution, and reproduction in any medium, provided you give appropriate credit to the original author(s) and the source, provide a link to the Creative Commons license, and indicate if changes were made.

parameter was also done by Young [3]. These studies invited multi-faceted analyses [4–17] of propagation of Newtonian fluid through constricting channels including factors of magnetic field, body acceleration and pulsatile nature of blood flow. Deshpande et al. [18] gave a new dimension to this investigation by developing a scheme to study Newtonian fluid flow through a stenosis that can be described axisymmetrically. How approximation of Reynolds number depending upon particular geometric facet of flow can alter the dynamics was discussed analytically by Smith [19].

Due to non-Newtonian characteristics of blood, many investigations were carried out to encompass these characteristics in flow modelling. In addition to inclusion of non-Newtonian behaviour of blood in propagation, structural limitations of stenosis were accommodated by considering various appropriate models such as power law, Herschel–Bulkley, Casson and Carreau models [20–33]. A study of blood rheology brings up thixotropic and viscoplastic nature of dense blood suspension, platelets, leucocytes, etc. These characteristics along with responses of blood cells to varying shear were analysed by Merill, Cokelet and Dintenfass [34–36]. Classification of appropriate models to describe blood flow through stenosis involving the aspect of particular structural aggregation in low-shear was done by Owens [37]. According to his experimental and theoretical results, non-Newtonian characteristics of blood were better projected by Herschel–Bulkley and Casson models. However, limitation of Casson model in a complete description of blood flow dynamics was brought up by Blair and Spanner [38]. The use of Herschel–Bulkley model to include many physiological characteristics of blood flow was adopted by Priyadharshini and Ponalgusamy [39, 40]. The factors of timed movement of channel due to peristaltic flow and tapering of the channel wall were studied by Mandal, Manton and Whitemore [41–43].

An elaborate analysis of thixotropic characteristic of blood was prepared [44, 45] by means of structural parameter, but Mewis and Wagner [46] studied the characteristics of yield stress and time-dependent viscosity by relating these with above structural parameter. This parameter time evolution was discussed in defining the characteristics of thixotropy. A study by Apostolidis and Beris [47] reflected on suitability of Casson model to describe the properties of thixotropy and viscoplasticity for low-shear rate flows, but its lack of encompassing the time-dependent viscosity as in colloidal blood suspension was already pointed out by Mewis [48].

The current investigation has also been inspired by an experimental study conducted by Apostolidis [47] in which he linked the characteristics of yield stress and thixotropy with a structural, time-evolving parameter. In addition to describing non-Newtonian characteristics of time-dependent viscosity of blood, this model's limiting results can help to validate available results in history. Here, we have prepared a theoretical analysis of unsteady blood flow though a stenosed artery with tapering described by a model such that this model's structural parameter is linked with yield stress and shear thinning of fluid in time. Following a recent analysis prepared by Apostolidis [49], we have chosen $[0, 1]$ as the range of structural parameter, and over this range, we have recorded variation in dynamics of flow. In addition to collecting analytical and numerical results regarding axial velocity, shear stress, flow rate and flow resistance with the help of chosen pressure gradient, we have pointed out a range of parameter variation that hints at our model's results being closer to experimental results than the results obtained by Herschel–Bulkley model.

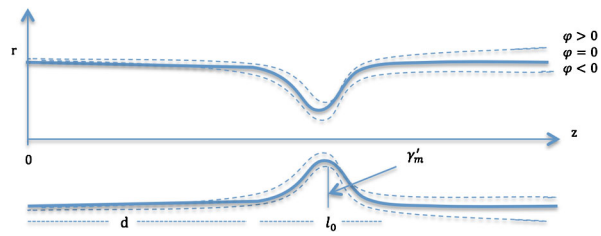

Figure 1 Two-dimensional stenosed and tapering channel

2 Geometry of flow in a tapered artery

A cylindrical coordinate system (r, θ, z) has been chosen to study dynamics of blood flow through an elastic tapered vessel with mild stenosis. We have considered z-axis to be in the direction of channel such that it is perpendicular to radius of channel, r to be in the direction of radius of a vessel (Fig. 1) and θ is taken along the circumferential direction. In order to model unsteady motion of a non-Newtonian fluid, we have considered a structural parameter modelling that is thixotropic modelling for incompressible fluid. The tapering of channel has been represented by an angle ϕ which is different from circumferential angle. The following geometric representation of artery with stenosis has been considered [41]:

$$\bar{R}(z,t) = \begin{cases} ((m'z + R_0) - \frac{\gamma_{m'} \sec\phi(z-d)}{\frac{l_0^2}{4} - \gamma_{m'}^2 \sin^2\phi}(l_0 - (z-d)))\bar{\eta}(t), & \text{for } d \le z \le d + l_0, \\ (m'z + R_0)\bar{\eta}(t), & \text{otherwise,} \end{cases} \tag{1}$$

where $\bar{R}(z,t)$ describes the radius of tapered artery. ϕ is taken as an angle of tapering where $\phi < 0$, $\phi > 0$ and $\phi = 0$ represent converging tapering, diverging tapering and no tapering, respectively. Also, d, R_0, l_0, $\gamma_{m'}$ and $m' = \tan\phi$ denote the position of stenosis, constant radius of non-tapered artery in the non-stenotic region, length of stenosis, height of stenosis at $z = d + \frac{l_0}{2}$ (no tapering) and slope of tapering, respectively.

In the above geometry, $\bar{\eta}(t)$ is defined as

$$\bar{\eta}(t) = 1 - g\{\cos(\omega t) - 1\}e^{-g\omega t},$$

where the constant g represents the amplitude of small oscillations and angular frequency is defined as $\omega = 2\pi f$ with f being the pulse frequency.

3 Mathematical formulation

The description of two-dimensional, axisymmetric flow has been made through the continuity equation and the governing equations of momentum for r and z components. These equations are

$$\rho\left(\frac{\partial u}{\partial t} + u\frac{\partial u}{\partial r} + w\frac{\partial u}{\partial z}\right) = -\left(\frac{1}{r}\frac{\partial(r\tau_{rr})}{\partial r} + \frac{\partial(\tau_{zr})}{\partial z}\right) - \frac{\partial p}{\partial r}, \tag{2}$$

$$\rho\left(\frac{\partial w}{\partial t} + u\frac{\partial w}{\partial r} + w\frac{\partial w}{\partial z}\right) = -\left(\frac{1}{r}\frac{\partial(r\tau_{rz})}{\partial r} + \frac{\partial(\tau_{zz})}{\partial z}\right) - \frac{\partial p}{\partial z}, \tag{3}$$

$$\frac{\partial u}{\partial r} + \frac{u}{r} + \frac{\partial w}{\partial z} = 0, \tag{4}$$

where $u = u(r,z,t)$, $w = w(r,z,t)$ and ρ represent radial component of velocity, axial component of velocity and density of incompressible fluid, respectively.

The constitutive equations are taken to be

$$\tau = \lambda\tau_y + (1-\lambda)\bar{k}(-\dot{\gamma})^n; \qquad \tau > \tau_y, \quad 0 < \lambda < 1, \tag{5}$$

where τ, $\dot{\gamma}$, τ_y, $\bar{k}$ and n denote shear stress, rate of deformation, yield stress, consistency index and flow behaviour index, respectively, along with $\tau = |\tau_{rz}| = -\tau_{rz}$.

The time-dependent thixotropic model (5) describes the flow of non-Newtonian fluids. Particularly, those fluids which are viscoplastic in nature and depend on deformation history for complete description of flow dynamics. The phenomenon of resting state of fluid under static condition and movement of particles under application of shear (change of viscosity) is completely enveloped in this model. This model encompasses the time-dependence variation of viscosity through the link of single structural parameter, λ. Also [50],

$$\dot{\gamma} = 0, \qquad \tau \le \tau_y \tag{6}$$

has been placed to ensure the continuation of flow for our considered model (5).

The boundary conditions chosen for our system are

$$w(r,z,t) = 0 \quad \text{at } r = \bar{R}(z,t); \qquad \tau_{rz}(r,z,t) = 0 \quad \text{at } r = 0. \tag{7}$$

Following the analysis of mechanism in human beings by Burton [51], pressure gradient has been considered in the given form

$$-\frac{\partial p}{\partial z} = A_0 + A_1\cos(\omega t), \quad t > 0, \tag{8}$$

where A_0 represents the constant amplitude of pressure gradient and A_1 helps to describe systolic and diastolic pressure, being amplitude of pulsatile component.

The following non-dimensional variables have been chosen:

$$\begin{aligned}
&w^* = \frac{w}{w_0}, \qquad u^* = \frac{u}{u_0}, \qquad t^* = \frac{w_0 t}{l}, \qquad z^* = \frac{z}{l}, \qquad p^* = \frac{p}{p_0},\\
&\tau_{rz}^* = \frac{R_0\tau_{rz}}{\mu w_0}, \qquad \tau_{zz}^* = \frac{l\tau_{zz}}{\mu w_0}, \qquad t_0 = \frac{l}{w_0}, \qquad w_0 = \frac{u_0 l}{R_0}, \qquad r^* = \frac{r}{R_0},\\
&d^* = \frac{d}{l}, \qquad l_0^* = \frac{l_0}{l}, \qquad \omega^* = \frac{t_0\omega}{2\pi}, \qquad p_0 = \frac{\mu l w_0}{R_0^2}, \qquad R^* = \frac{\bar{R}}{R_0},\\
&m = \frac{m' l}{R_0}, \qquad \gamma_{m'}^* = \frac{\gamma_{m'}}{R_0}, \qquad R_e = \frac{\rho R_0 w_0}{\mu}, \qquad Q^* = \frac{\bar{Q}}{w_0 R_0^2},\\
&A_0^* = \frac{A_0 R_0^2}{\mu w_0}, \qquad A_1^* = \frac{A_1 R_0^2}{\mu w_0}, \qquad \tau_y^* = \frac{R_0\tau_y}{\mu w_0}, \qquad K = \frac{\bar{k}}{\mu}\left(\frac{w_0}{R_0}\right)^{n-1},
\end{aligned} \tag{9}$$

where w_0 and u_0 are characteristic scales.

Simplification of our system is reached using non-dimensional quantities (9), very small Reynolds number, R_e, and

$$R_0 \ll l,$$

where l is the finite length of artery. Thus, we obtain (ignoring *)

$$-\frac{\partial p}{\partial z} = \frac{1}{r}\frac{\partial(r\tau_{rz})}{\partial r}, \tag{10}$$

$$\frac{\partial p}{\partial r} = 0, \tag{11}$$

$$\tau = \lambda\tau_y + (1-\lambda)K\left(-\frac{\partial w}{\partial r}\right)^n, \tag{12}$$

$$-\frac{\partial p}{\partial z} = A_0 + A_1\cos(2\pi\omega t), \quad t > 0. \tag{13}$$

And the boundary conditions are

$$w(r,z,t) = 0, \quad r = R(z,t); \qquad \tau_{rz}(r,z,t) = 0, \quad r = 0. \tag{14}$$

Now the geometry of the wall will be presented as

$$R(z,t) = \left\{(mz+1) - \frac{4\gamma_m \sec\phi(z-d)(l_0-(z-d))}{l_0^2}\right\}\eta(t), \tag{15}$$

for $d \le z \le d + l_0$, where

$$\eta(t) = 1 - g\left\{\cos(2\pi\omega t) - 1\right\}e^{-2\pi g\omega t}. \tag{16}$$

4 Analytical expressions of velocity, shear stress and flow rate

$x = \frac{r}{R(z,t)}$ has been used to make a coordinate transformation, and we obtain from Eqs. (10), (11), (12) and (14) the following:

$$-\frac{\partial p}{\partial z} = \frac{1}{xR(z,t)}\frac{\partial(x\tau_{xz})}{\partial x}, \tag{17}$$

$$-\frac{\partial p}{\partial x} = 0, \tag{18}$$

$$\tau = \lambda\tau_y + \frac{(1-\lambda)K}{R^n(z,t)}\left(-\frac{\partial w}{\partial x}\right)^n \tag{19}$$

with boundary conditions

$$w(x,z,t) = 0 \quad \text{at } x = 1; \qquad \tau_{xz}(x,z,t) = 0 \quad \text{at } x = 0. \tag{20}$$

We also have

$$\frac{\partial w}{\partial x} = 0, \quad 0 \le x \le R_{\mathrm{pc}}, \tag{21}$$

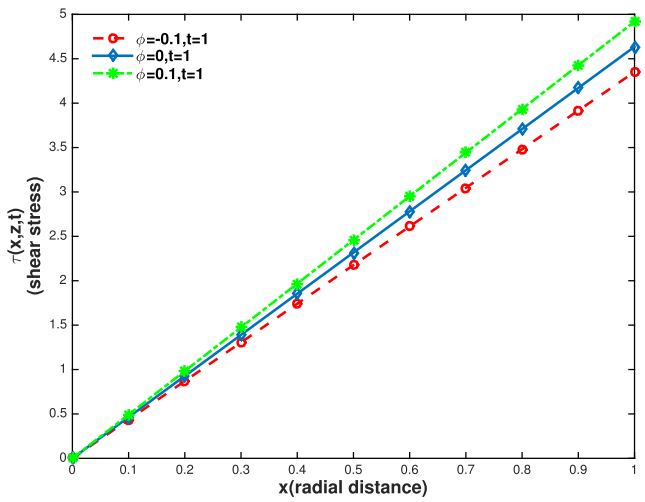

Figure 2 Shear stress vs radial distances for $\phi = -0.1, 0, 0.1$ at $z = 28$, $t = 1$, $\tau_y = 0.4$, $K = 1.6$

where R_{pc} is the radius of plug core region.

With the help of Eqs. (17) and (18), we can write pressure as a function of only an axial coordinate, that is,

$$p = p(z). \tag{22}$$

Solving Eq. (17) with $(20)_2$ and (22), we obtain an expression of shear stress

$$\tau_{xz} = \frac{xR(z,t)}{2}\left(-\frac{\partial p}{\partial z}\right). \tag{23}$$

And the expression for wall shear stress ($x = 1$) is

$$\tau_{\mathrm{ws}} = \frac{R(z,t)}{2}\left(-\frac{\partial p}{\partial z}\right). \tag{24}$$

Solving Eq. (19) with $(20)_1$ and (23), we get an expression for axial velocity

$$\begin{aligned} w(x,z,t) = {} & \frac{nR(z,t)}{(n+1)(M+2\lambda\tau_y)(2K(1-\lambda))^{\frac{1}{n}}} \\ & \times \left\{M^{\frac{n+1}{n}} - \left(Mx + 2\lambda\tau_y(x-1)\right)^{\frac{n+1}{n}}\right\}, \end{aligned} \tag{25}$$

where $M = R(z,t)(-\frac{\partial p}{\partial z}) - 2\lambda\tau_y$ and $R_{\mathrm{pc}} \le x \le R(z,t)$.

And the velocity in the plug core region is

$$w_{\mathrm{pc}}(x,z,t) = \frac{nR(z,t)}{(n+1)(M+2\lambda\tau_y)(2K(1-\lambda))^{\frac{1}{n}}}\left\{M^{\frac{n+1}{n}}\right\} \tag{26}$$

for $0 < x \le R_{\mathrm{pc}}$ and $R_{\mathrm{pc}} = \frac{2\lambda\tau_y}{R(z,t)\frac{-\partial p}{\partial z}}$.

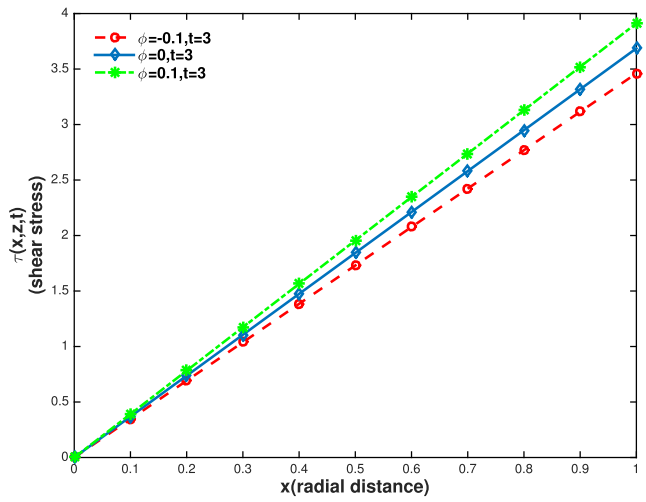

Figure 3 Shear stress vs radial distances for $\phi = -0.1, 0, 0.1$ at $z = 28$, $t = 3$, $\tau_y = 0.4$, $K = 1.6$

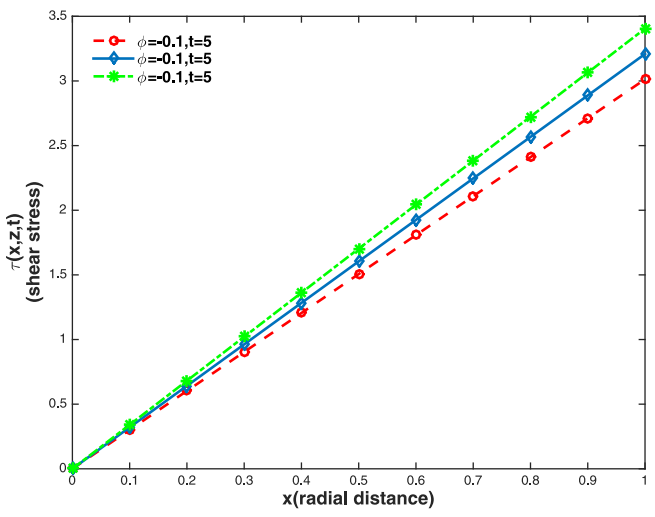

Figure 4 Shear stress vs radial distances for $\phi = -0.1, 0, 0.1$ at $z = 28$, $t = 5$, $\tau_y = 0.4$, $K = 1.6$

Volume flow rate is defined as

$$\bar{Q} = 2\pi \int_{r=0}^{r=\bar{R}(z,t)} rw(r,z,t)\,dr \tag{27}$$

which in non-dimensional form (ignoring $*$) can be written as

$$Q(z,t) = 2\pi \int_{r=0}^{r=R(z,t)} rw(r,z,t)\,dr. \tag{28}$$

Equation (28) in terms of x coordinate is

$$Q(z,t) = 2\pi R^2(z,t) \int_0^1 xw(x,z,t)\,dx. \tag{29}$$

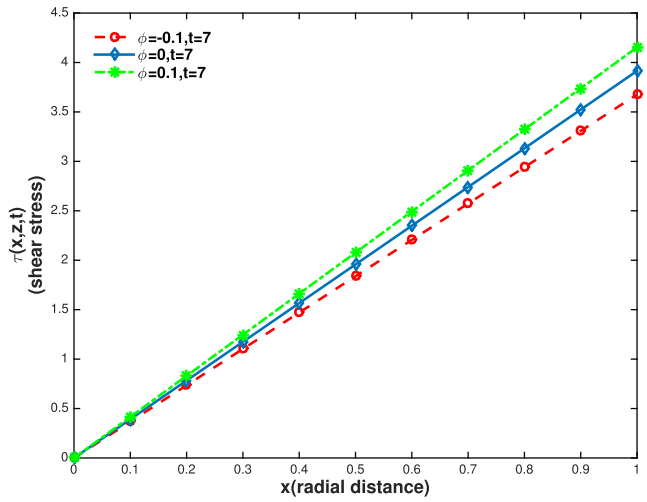

Figure 5 Shear stress vs radial distances for $\phi = -0.1, 0, 0.1$ at $z = 28$, $t = 7$, $\tau_y = 0.4$, $K = 1.6$

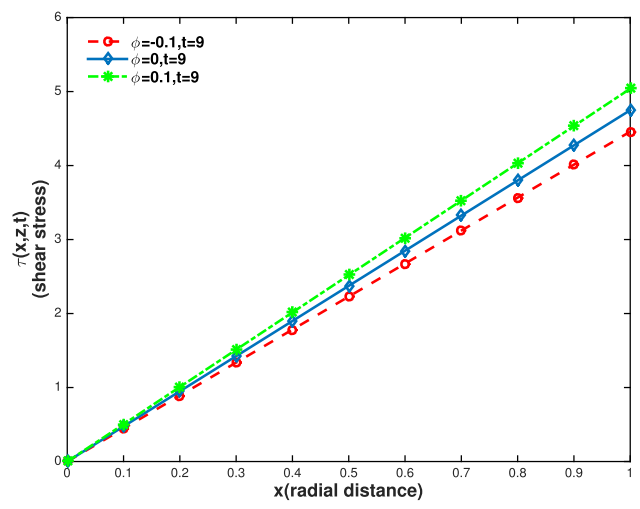

Figure 6 Shear stress vs radial distances for $\phi = -0.1, 0, 0.1$ at $z = 28$, $t = 9$, $\tau_y = 0.4$, $K = 1.6$

Equation (29) can be simplified using Eqs. (25) and (26). Thus, we obtain

$$\begin{aligned} Q(z,t) = {} & \frac{\pi n R^3(z,t)}{(2n^2+3n+1)(3n+1)(M+2\lambda\tau_y)^3(2K(1-\lambda))^{\frac{1}{n}}} \\ & \times \Big\{(n+1)(2n+1)M^{\frac{3n+1}{n}} \\ & + 4\lambda\tau_y(n+1)(3n+1)M^{\frac{2n+1}{n}} \\ & + 4\lambda^2\tau_y^2(2n+1)(3n+1)M^{\frac{n+1}{n}}\Big\}, \end{aligned} \tag{30}$$

where $M = R(z,t)(-\frac{\partial p}{\partial z}) - 2\lambda\tau_y$.

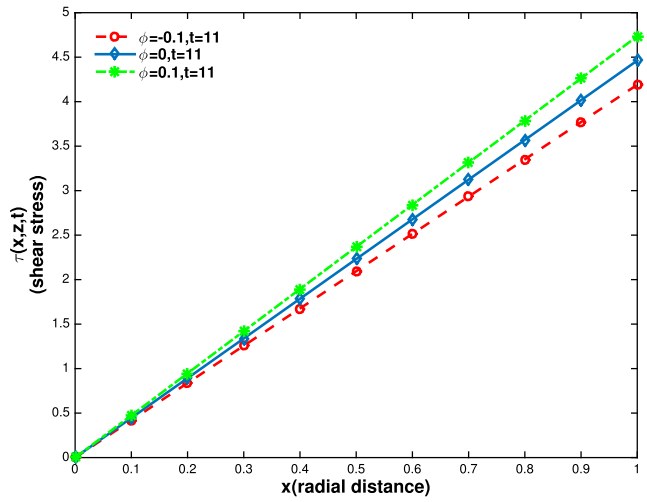

Figure 7 Shear stress vs radial distances for $\phi = -0.1, 0, 0.1$ at $z = 28$, $t = 11$, $\tau_y = 0.4$, $K = 1.6$

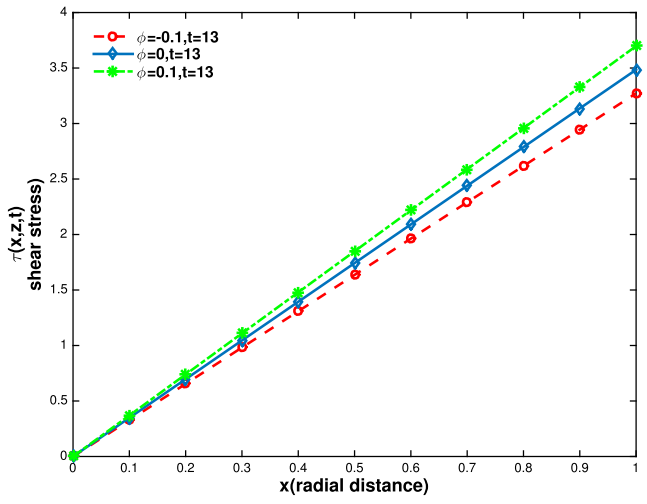

Figure 8 Shear stress vs radial distances for $\phi = -0.1, 0, 0.1$ at $z = 28$, $t = 13$, $\tau_y = 0.4$, $K = 1.6$

For a given time, resistance to flow can be obtained using

$$\mho = \int_0^z \frac{(-\frac{\partial p}{\partial z})}{Q}\, dz \tag{31}$$

with the help of Eqs. (13) and (30).

Table 1 has been constructed to get an estimate of the values of axial velocity corresponding to λ-variation for converging tapering at a given position of stenosis and time.

Table 1 Values of axial velocity $w(x,z,t;\lambda)$ resulting from Eq. (25) corresponding to λ-values for $\phi = -0.1$, $t = 0.45$ and $z = 28$

x	0.6	0.7	0.8	0.9	1
$w(x,z,t;0)$	1.071	0.879	0.639	0.347	0
$w(x,z,t;0.1)$	1.242	1.020	0.742	0.404	0
$w(x,z,t;0.2)$	1.467	1.206	0.879	0.478	0
$w(x,z,t;0.3)$	1.776	1.462	1.066	0.581	0
$w(x,z,t;0.4)$	2.220	1.829	1.335	0.728	0
$w(x,z,t;0.5)$	2.900	2.392	1.747	0.953	0
$w(x,z,t;0.6)$	4.037	3.334	2.437	1.331	0
$w(x,z,t;0.7)$	6.217	5.138	3.760	2.055	0
$w(x,z,t;0.8)$	11.507	9.521	6.974	3.815	0
$w(x,z,t;0.9)$	33.402	27.669	20.286	11.109	0

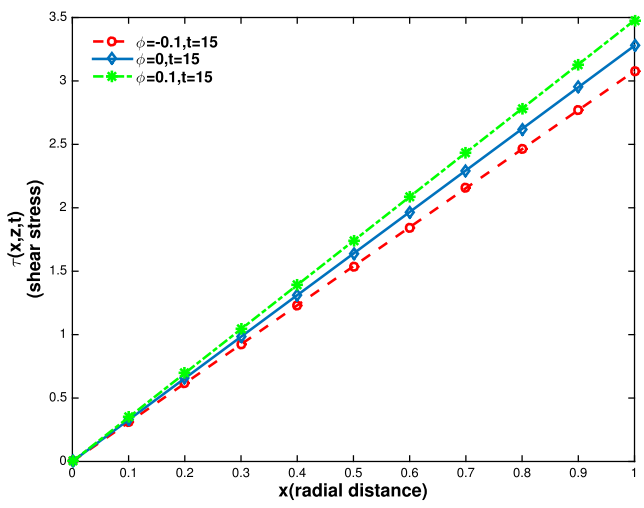

Figure 9 Shear stress vs radial distances for $\phi = -0.1, 0, 0.1$ at $z = 28$, $t = 15$, $\tau_y = 0.4$, $K = 1.6$

5 Discussion

In order to get validation for results corresponding to approximation of our modelling parameter, we have considered the following numerical values [41]:

$$\gamma_m = 0.2, \qquad l_0 = 16, \qquad d = 20, \qquad l = 50, \qquad \omega = 6, \qquad g = 0.1,$$
$$n = 0.639, \qquad R_0 = 0.8.$$

In Figs. 2–9, time-dependent shear stress has been plotted against radial distances at a given position of stenosis, $z = 28$, and varying time in the range $t \in [1, 15]$. These graphs show consistent increase in shear stress such that it reaches its maximum value on the boundary wall ($x = 1$). Also it is noted that shear stress is higher for the case of diverging tapering in comparison to the cases of converging and no tapering. In these images, observing the wall shear stress, $\tau_{ws}(x,z,t)$ ($x = 1$) (say for diverging tapering) data points show that shear stress decreases initially ($t \in [1, 5]$), starts increasing ($t \in (5, 9]$), decreases again ($t \in (9, 15]$) and the cycle goes on, concluding that shear stress varies in an oscillating pattern. The oscillations in shear stress correspond to relaxing and constricting movement of a vessel with change in time.

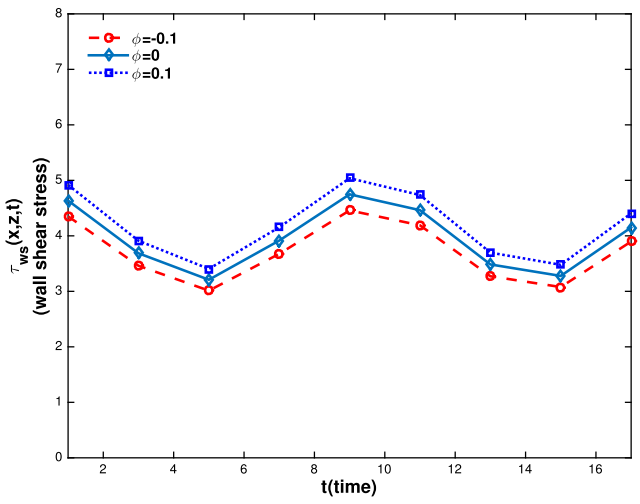

Figure 10 Wall shear stress vs time for $\phi = -0.1, 0, 0.1$ at $z = 28$, $\tau_y = 0.4$, $K = 1.6$

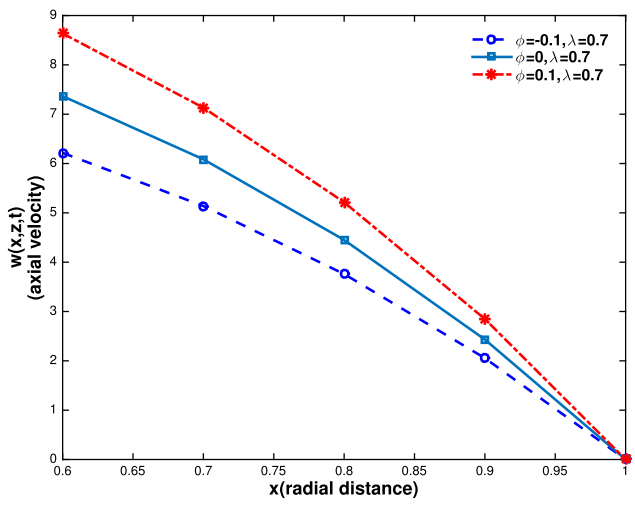

Figure 11 Axial velocity vs radial distances for $\phi = -0.1, 0, 0.1$ at $z = 28$, $t = 0.45$, $\tau_y = 0.4$, $K = 1.6$, $\lambda = 0.7$

A clear image of oscillating pattern of wall shear stress variation in response to change in time has also been presented in Fig. 10 for the cases of converging, diverging and no-tapering. Figures 11–13 represent variation in axial velocity corresponding to changes in near-wall radial distances. It is observed that the axial velocity continues to decrease in such a way that it reaches zero on the wall vessel ($x = 1$), satisfying the no-slip boundary condition. It is also noted that the magnitude of axial velocity for diverging tapering is higher than that for the cases of converging and no-tapering. It is due to the fact that diverged opening in the neighbourhood of stenosis provides a way for fluid to propagate with higher speed, comparatively. An analysis of axial velocity dependence on thixotropic parameter λ was also made through these graphs. It shows that the axial velocity decreases for decreasing values of λ. Thus, in a theoretical scheme, the higher values of λ can play a

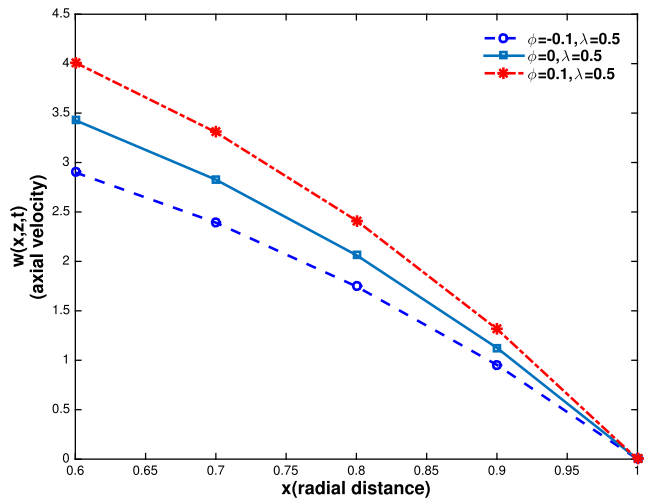

Figure 12 Axial velocity vs radial distances for $\phi = -0.1, 0, 0.1$ at $z = 28$, $t = 0.45$, $\tau_y = 0.4$, $K = 1.6$, $\lambda = 0.5$

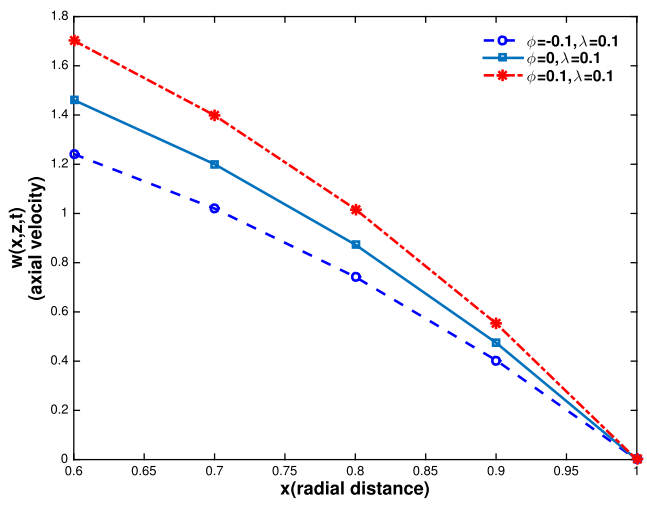

Figure 13 Axial velocity vs radial distances for $\phi = -0.1, 0, 0.1$ at $z = 28$, $t = 0.45$, $\tau_y = 0.4$, $K = 1.6$, $\lambda = 0.1$

role in increasing the magnitude of axial velocity that can be used in further implementation of model in the construction of an implanted vascular system.

We have made a comparison of axial velocity profiles in Figs. 14–16 for power law fluid, Newtonian fluid and thixotropic fluid (for some different values of λ). In response to changing radial distances, near the boundary wall, velocity is decreasing and reaching zero on the vessel wall. For all the cases of converging, diverging and no-tapering, we have made a note of increasing velocity for increasing values of λ. Interestingly, the velocity for power law fluid attains values smaller than thixotropic velocity for $\lambda = 0.1$, indicating the phenomenological differences of both models in regards to describing the viscosity and viscoplasticity levels. The lower magnitude of velocity for power law fluid also points to its lesser viscosity (in comparison to thixotropic fluid for $\lambda = 0.1$) that needed lesser pressure-gradient for flow propagation, which resulted in higher magnitude of velocity

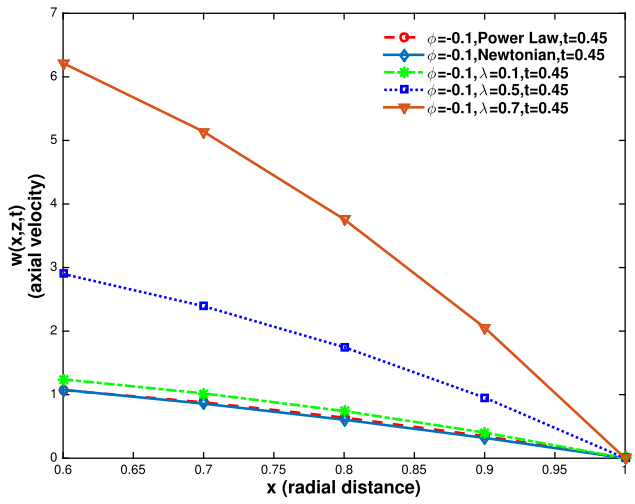

Figure 14 Axial velocity vs radial distances (near wall) for $\phi = -0.1$, $\lambda = 0.1, 0.5, 0.7$ at $z = 28$, $t = 0.45$, $\tau_y = 0.4$, $K = 1.6$, Power Law model ($\lambda \to 0$) and Newtonian fluid ($\lambda \to 0$, $\bar{K} = 0.035$, $n = 1$)

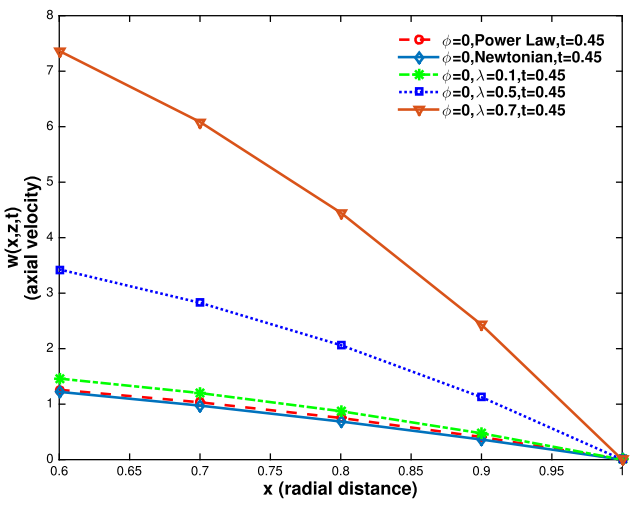

Figure 15 Axial velocity vs radial distances (near wall) for $\lambda = 0.1, 0.5, 0.7$ and $\phi = 0$ at $z = 28$, $t = 0.45$, $\tau_y = 0.4$, $K = 1.6$, power law model ($\lambda \to 0$) and Newtonian fluid ($\lambda \to 0$, $\bar{K} = 0.035$, $n = 1$)

for $\lambda = 0.1$ level fluid. An observation of lowest profiles of Newtonian fluid is also made in all Figs. 14–16, validating the lowest pressure gradient required for Newtonian fluid flow. The lowest-velocity-magnitude profiles for Newtonian fluid is more apparent in diverging tapering case (Fig. 16). The lowest magnitude of velocity for power law fluid in comparison to thixotropic fluid ($\lambda = 0.1, 0.5, 0.7$) velocity also corroborates the available results in non-Newtonian fluid modelling [41]. It can be seen that velocity for all models attains higher values for diverging tapering in comparison to no-tapering and converging tapering, the latter being smallest in terms of magnitude.

In Figs. 17–19, we have plotted flow resistance against time for the case of converging tapering. It is observed that the resistance to flow increases in the beginning of a cycle at the position of stenosis due to propagation of fluid through constriction and then it starts

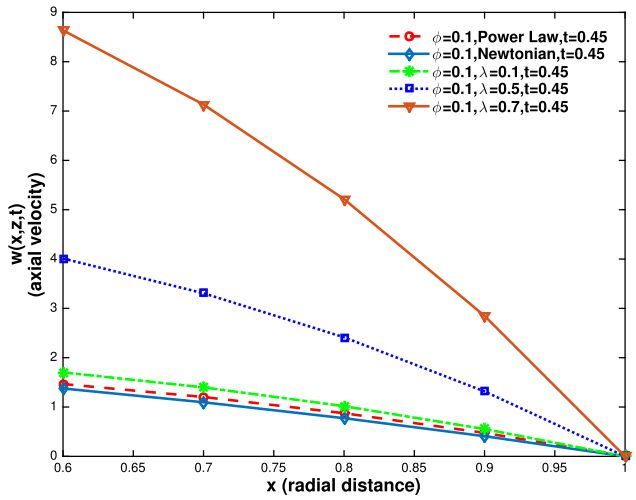

Figure 16 Axial velocity vs radial distances (near wall) for $\phi = 0.1$, $\lambda = 0.1, 0.5, 0.7$ at $z = 28$, $t = 0.45$, $\tau_y = 0.4$, $K = 1.6$, power law model ($\lambda \to 0$) and Newtonian fluid ($\lambda \to 0$, $\bar{K} = 0.035$, $n = 1$)

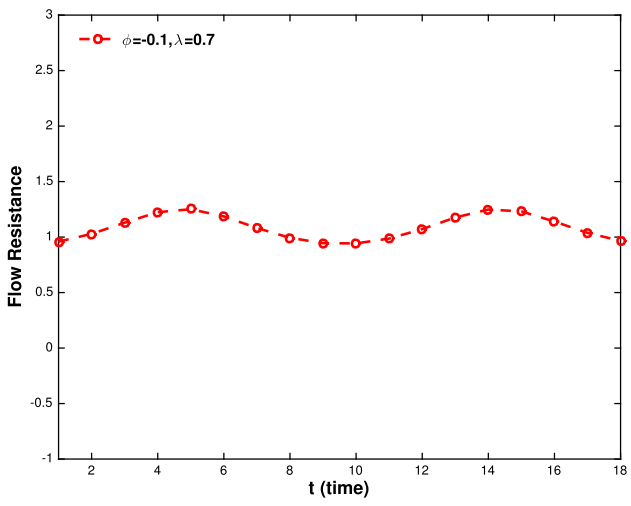

Figure 17 Flow resistance vs time for $\phi = -0.1$ at $z = 28$, $\tau_y = 0.4$, $K = 1.6$, $\lambda = 0.7$

decreasing for the relaxation part of the cycle. The continuation of cyclic movement of flow resistance with time leads to an oscillating pattern depicted in graphs. It is interesting to observe that resistance to flow increases for smaller values of λ and decreases for larger values of λ.

Figures 20–22 express the flow rate tendency to change in response to varying pressure gradient for the cases of converging, diverging and no-tapering. It is interesting to note that the rate of increase in flow rate for rising pressure-gradient is non-linear for thixotropic fluid unlike the established results in history. However, the flow rate profile for converging tapering is almost linear. A direct relation between flow rate and thixotropic parameter λ has also been observed here for the same values of pressure-gradient.

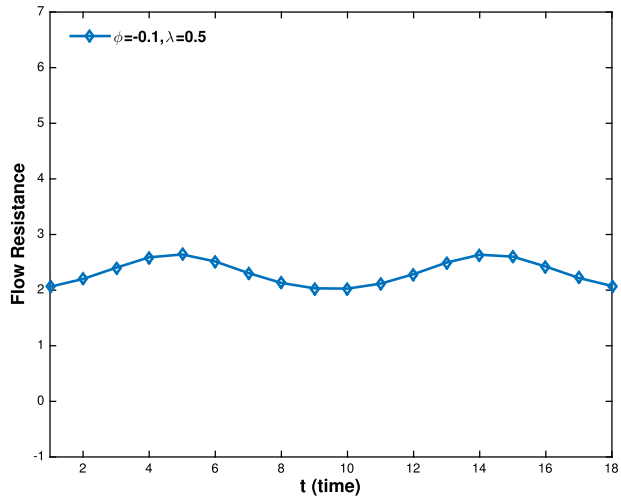

Figure 18 Flow resistance vs time for $\phi = -0.1$ at $z = 28$, $\tau_y = 0.4$, $K = 1.6$, $\lambda = 0.5$

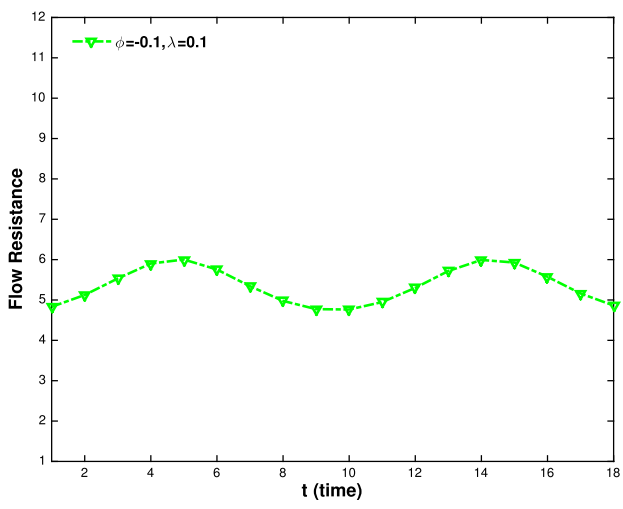

Figure 19 Flow resistance vs time for $\phi = -0.1$ at $z = 28$, $\tau_y = 0.4$, $K = 1.6$, $\lambda = 0.1$

In Figs. 23–25, we have investigated the response of axial velocity against radial distances for varying yield stress τ_y and for the case of converging tapering. These graphs show that the axial velocity decreases for rising values of yield stress in corroboration with phenomenal results of higher-yield stress fluid being subject to higher resistance in comparison to lower-yield stress fluid. It is interesting to note that, for smaller values of λ (say $0.1 < \lambda < 0.5$), not only the axial velocity curve mutual separation is decreasing, but also for very small values (say $\lambda = 0.1$) near the wall of a vessel, the profiles seem to be coinciding. A direct relation of axial velocity and parametric value of λ is also verified as in the case of one-value yield stress fluid.

The analysis of variation flow rate with respect to time has been done through graphs. We have obtained the profiles for flow rate at the position of stenosis, $z = 28$, and for the cases of converging, diverging and no-tapering. In Figs. 26–28, flow rate has been observed

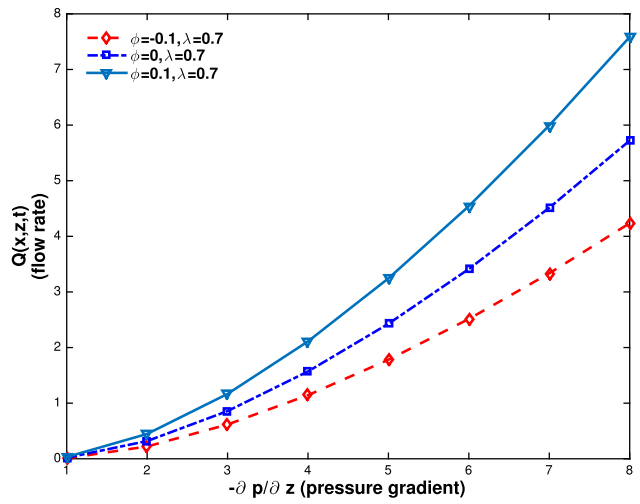

Figure 20 Flow rate vs pressure gradient for $\phi = -0.1, 0, 0.1$ at $z = 28$, $t = 0.45$, $\tau_y = 0.4$, $K = 1.6$, $\lambda = 0.7$

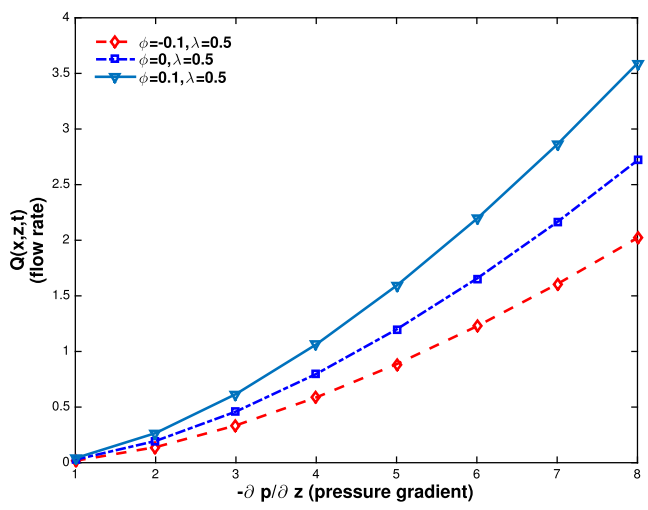

Figure 21 Flow rate vs pressure gradient for $\phi = -0.1, 0, 0.1$ at $z = 28$, $t = 0.45$, $\tau_y = 0.4$, $K = 1.6$, $\lambda = 0.5$

to follow an oscillating pattern with respect to time. It is also noted that flow rate assumes higher magnitude for diverging tapering in comparison to no-tapering. Also, due to constriction of the channel at the position of stenosis, $z = 28$, flow rate for converging tapering assumes smallest magnitude with varying time. These figures also reflect on the influence of thixotropic parameter λ on flow rate. It can be observed that flow rate decreases for smaller values of λ.

6 Conclusions

The following conclusions have been reached regarding the study of propagation of blood through a stenosed channel with tapering. How a structural parameter and timed movement of vessel influence dynamics and validation of some of available results has also been

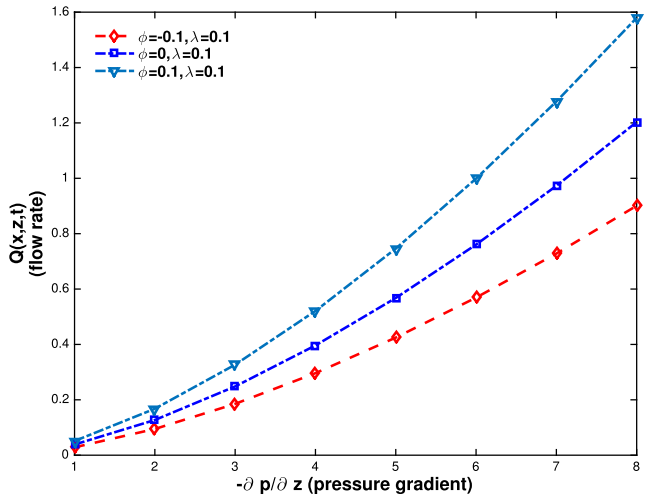

Figure 22 Flow rate vs pressure gradient for $\phi = -0.1, 0, 0.1$ at $z = 28$, $t = 0.45$, $\tau_y = 0.4$, $K = 1.6$, $\lambda = 0.1$

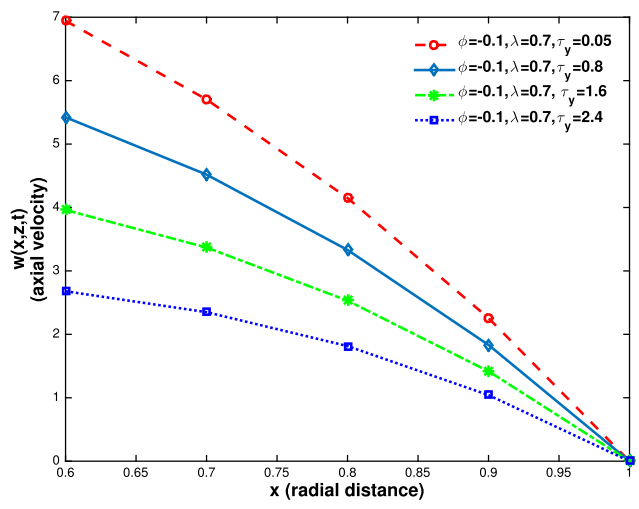

Figure 23 Axial velocity vs radial distances (near wall) for varying yield stress at $z = 28$, $t = 0.45$, $K = 1.6$, $\phi = -0.1$, $\lambda = 0.7$

recorded here with the help of analytical and numerical analysis. These salient points are as follows:

1. At given stenosis position and time, shear stress continues to increase with increasing radial distances, attaining its maximum value on a boundary wall of the vessel. Shear stress assumes higher magnitudes for diverging tapering due to comparatively higher influx of fluid in a diverged part of the channel.
2. The oscillating movement of shear stress (or wall shear stress) with time owes its pattern to the nature of pressure gradient in particular and the wall movement of the vessel in general.
3. In a manner of verifying the no-slip boundary condition, the response of axial velocity was recorded for near-wall radial distance changes. In addition to

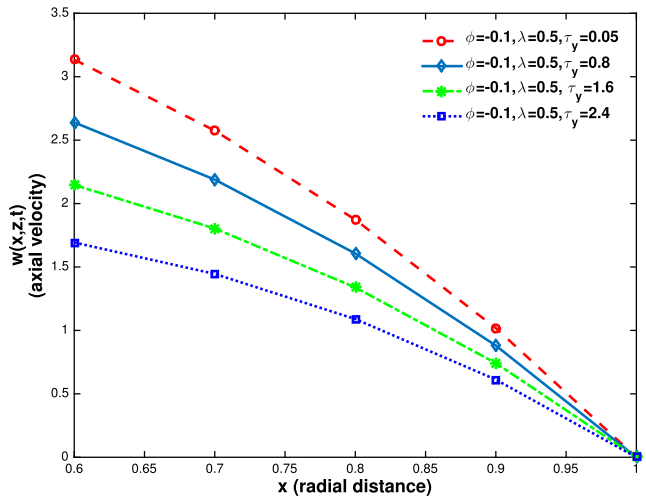

Figure 24 Axial velocity vs radial distances (near wall) for varying yield stress at $z = 28$, $t = 0.45$, $K = 1.6$, $\phi = -0.1$, $\lambda = 0.5$

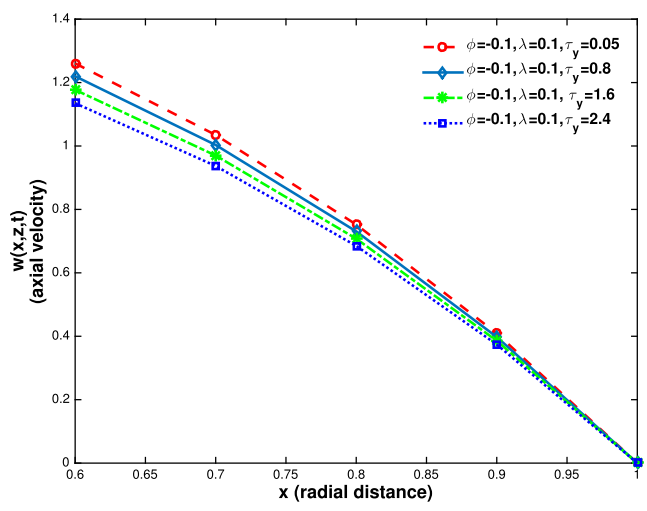

Figure 25 Axial velocity vs radial distances (near wall) for varying yield stress at $z = 28$, $t = 0.45$, $K = 1.6$, $\phi = -0.1$, $\lambda = 0.1$

continuous drop in axial velocity while approaching boundary wall, the velocity magnitude is higher for diverging tapering as fluid endures lesser hindrance in its propagation in a widening channel.

4. The magnitude of axial velocity at a given radial distance drops for decreasing values of thixotropic parameter λ $(0 < \lambda < 1)$.
5. The study of comparative profiles of axial velocity for Newtonian, power law and thixotropic fluid $(\lambda = 0.1, 0.5, 0.7)$ reflects on two interesting phenomena. The first being the occurrence of lower profile of axial velocity for power law fluid among non-Newtonian fluids, matching with available theoretical results and obtaining lowest-magnitude-velocity profile for Newtonian fluid being the second one. The first fact describes that the thixotropic fluid for $\lambda = 0.1$ encounters more resistance

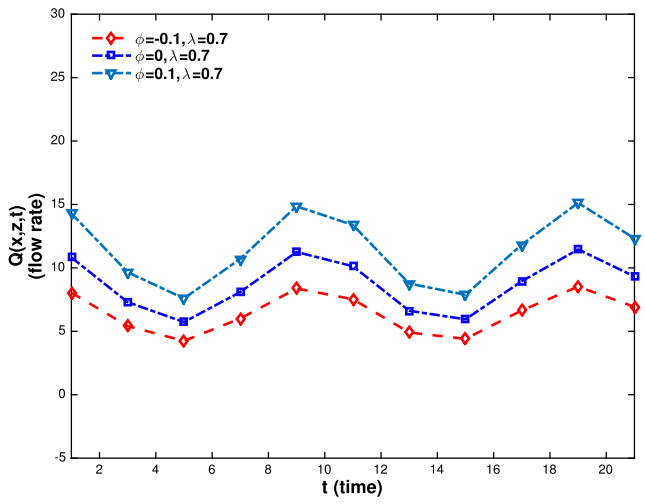

Figure 26 Flow rate vs time for $\phi = -0.1, 0, 0.1$ at $z = 28$, $\tau_y = 0.4$, $K = 1.6$, $\lambda = 0.7$

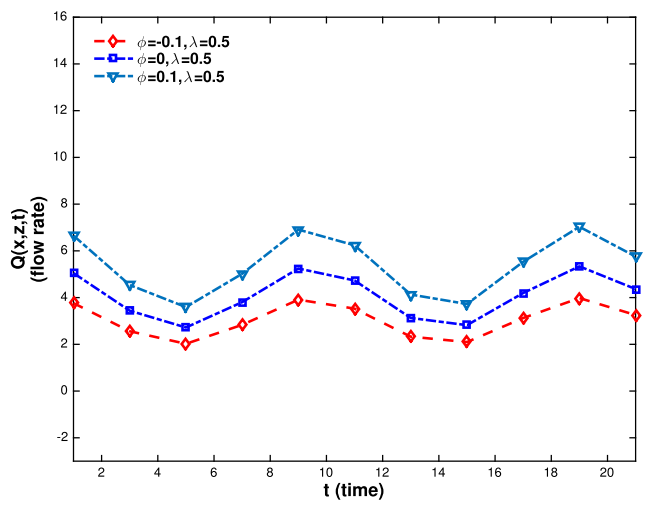

Figure 27 Flow rate vs time for $\phi = -0.1, 0, 0.1$ at $z = 28$, $\tau_y = 0.4$, $K = 1.6$, $\lambda = 0.5$

in its propagation than power law and Newtonian fluids. Also, axial velocity increases for increasing values of λ.

6. The comparison of axial velocity profiles for different models here with theoretical and experimental values of axial velocity profile for Herschel–Bulkley fluid model [39] reflects on the possibility for the latter to coincide with thixotropic fluid profile for $0.6 \leq \lambda \leq 0.8$. Thus, it would be interesting to further investigate flow properties of thixotropic fluid for $0.8 < \lambda < 1$, treating a thixotropic fluid model different from Herschel–Bulkley fluid model.
7. For converging tapering, resistance to flow follows an oscillating pattern with time in accordance with oscillating variation in pressure gradient.
8. The resistance to flow decreases for larger values of λ, verifying the fact here that axial velocity increases for larger values of λ.

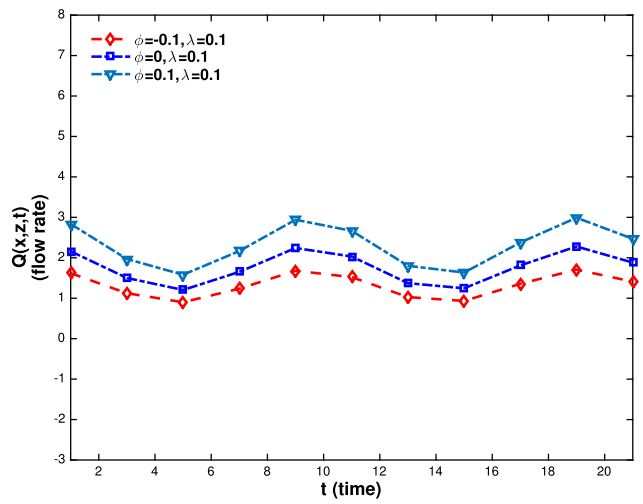

Figure 28 Flow rate vs time for $\phi = -0.1, 0, 0.1$ at $z = 28$, $\tau_y = 0.4$, $K = 1.6$, $\lambda = 0.1$

9. Flow rate increases with increase in pressure gradient. This increase is represented by slight parabolic curves for diverging and no tapering unlike the available results for Newtonian and non-Newtonian fluids. However, the increase in flow rate with rising pressure gradient for converging tapering is almost linear.
10. Flow rate assumes higher values for diverging tapering in comparison to no-tapering and converging tapering, respectively.
11. Flow rate has a direct relation to parametric value λ in validation with the results here that flow resistance increases for smaller λ-values and vice-versa.
12. For converging tapering, axial velocity decreases for increasing values of yield stress τ_y and its response to λ is observed to be direct.
13. As λ assumes values near zero, axial velocity response to varying yield stress gets considerably smaller. This phenomenon is apparent in axial velocity profiles for $\lambda = 0.1$.
14. Owing to rise and drop of pressure gradient, flow rate varies in oscillations with time, assuming a direct relation with λ.

Acknowledgements
The author thanks Dr. Howard Stone and Dr. Bhargav Rallabandi from the Department of Mechanical and Aerospace Engineering, Princeton University for their insightful discussions on the topic and Princeton University for providing a wonderful working atmosphere for completion of this project.

Funding
No funding was obtained or used for completion of this work.

Availability of data and materials
Not applicable.

Competing interests
The author declares that there are no competing interests in regards with the current article.

Authors' contributions
This entire work has been completed by the author, Dr. Nazish Shahid. Analytical solutions were determined by her and matching simulations were completed by her as well as graphical analysis through graphs had also been prepared by her. The author read and approved the final manuscript.

Publisher's Note

Springer Nature remains neutral with regard to jurisdictional claims in published maps and institutional affiliations.

Received: 24 January 2018 Accepted: 17 May 2018 Published online: 29 May 2018

References

1. Young, D.F.: Fluid mechanics of arterial stenoses. J. Biomech. Eng. **101**(3), 157–175 (1979). https://doi.org/10.1115/1.3426241
2. Young, D.F., Tsai, F.Y.: Flow characteristics in models of arterial stenoses: I. Steady flow. J. Biomech. **6**(4), 395–410 (1973)
3. Young, D.F.: Effect of a time dependent stenosis of flow through a tube. J. Eng. Ind. **90**, 248–254 (1968)
4. Misra, J.C., Chakravarty, S.: Flow in arteries in the presence of stenosis. J. Biomech. **19**, 907–918 (1986)
5. Tu, C., Deville, M., Dheur, L., Vandershuren, L.: Finite element simulation of pulsatile flow through arterial stenosis. J. Biomech. **25**, 1141–1152 (1992)
6. Belardinelli, E., Cavalcanti, S.: A new nonlinear two-dimensional model of blood motion in tapered and elastic vessels. Comput. Biol. Med. **21**, 1–13 (1991)
7. Nerem, R.E.: Vascular fluid mechanics, the arterial wall and arteriosclerosis. J. Biomech. Eng. Trans. ASME **114**, 274–282 (1992)
8. Cavalcanti, S.: Hemodynamics of an artery with mild stenosis. J. Biomech. **28**, 387–399 (1995)
9. Siouffi, M., Deplano, V., Pelissra, R.: Experimental analysis of unsteady flows through a stenosis. J. Biomech. **31**, 11–19 (1997)
10. Zendehboodi, G.R., Moayeri, M.S.: Comparison of physiological and simple pulsatile flows through stenosed arteries. J. Biomech. **32**, 959–965 (1999)
11. Chakravarty, S., Mandal, P.K.: Two-dimensional blood flow through tapered arteries under stenotic conditions. Int. J. Non-Linear Mech. **35**, 779–793 (2000)
12. Elshehawey, E.F., Elbarbary, E.M.E., Afifi, N.A.S., El-Shahed, M.: Pulsatile flow of blood through a porous medium under periodic body acceleration. Int. J. Theor. Phys. **39**(1), 183–188 (2000). https://doi.org/10.1023/A:1003611604207
13. Long, Q., Ku, X.Y., Ramnarine, K.V., Hoskins, P.: Numerical investigation of physiologically realistic pulsatile flow through arterial stenosis. J. Biomech. **34**, 1229–1242 (2001)
14. El-Shahed, M.: Pulsatile flow of blood through a stenosed porous medium under periodic body acceleration. Appl. Math. Comput. **138**(2–3), 479–488 (2003). https://doi.org/10.1016/S0096-3003(02)00164-9
15. Ponalagusamy, R., Tamil, R.T., Banerjee, A.K.: Mathematical model of pulsatile flow of non-Newtonian fluid in tubes of varying cross-sections and its implications to blood flow. J. Franklin Inst. **349**(5), 1681–1698 (2012)
16. Sharma, M.K., Bansal, K., Bansal, S.: Pulsatile unsteady flow of blood through porous medium in a stenotic artery under the influence of transverse magnetic field. Korea Australia Rheol. J. **24**(3), 181–189 (2012)
17. Ponalagusamy, R., Priyadharshini, S.: Nonlinear model on pulsatile flow of blood through a porous bifurcated arterial stenosis in the presence of magnetic field and periodic body acceleration. Comput. Methods Programs Biomed. **142**(5), 31–41 (2017)
18. Deshpande, M.D., Giddens, P.D., Mabon, F.R.: Steady laminar flow through modelled vascular stenoses. J. Biomech. **9**, 165–174 (1976)
19. Smith, F.T.: The separation flow through a severely constricted symmetric tube. J. Fluid Mech. **90**, 725–754 (1979)
20. Liepsch, D., Moravec, S.T.: Pulsatile flow of non-Newtonian fluid in distensible models of human arteries. Biorheology **21**, 571–586 (1984)
21. Chaturani, P., Samy, R.P.: A study of non-Newtonian aspects of blood flow through stenosed arteries and its applications in arterial diseases. Biorheology **22**, 521–531 (1985)
22. Theodorou, G., Bellet, D.: Laminar flows of a non-Newtonian fluid in mild stenosis. Comput. Methods Appl. Mech. Eng. **54**, 111–123 (1986)
23. Nakamura, M., Swada, T.: Numerical study on the flow of a non-Newtonian fluid through an axisymmetric stenosis. J. Biomech. Eng. Trans. ASME **110**, 137–143 (1988)
24. Nakamura, M., Swada, T.: Numerical study on the unsteady flow of non-Newtonian fluid. J. Biomech. Eng. Trans. ASME **112**, 100–103 (1990)
25. Pak, B., Cho, Y.I., Choi, S.U.S.: Separation and re-attachment of non-Newtonian fluid flows in a sudden expansion pipe. J. Non-Newton. Fluid Mech. **37**, 175–199 (1990). https://doi.org/10.1016/0377-0257(90)90004-U
26. Gopalan, N.P., Ponnalagarsamy, R.: Investigation on laminar flow of a suspension in corrugated straight tubes. Int. J. Eng. Sci. **30**, 631–644 (1992)
27. Misra, J.C., Patra, M.K., Misra, S.C.: A non-Newtonian fluid model for blood flow through arteries under stenotic conditions. J. Biomech. **26**, 1129–1141 (1993)
28. Tu, C., Deville, M.: Pulsatile flow of non-Newtonian fluid through arterial stenosis. J. Biomech. **29**, 899–908 (1996)
29. Das, B., Johnson, P.C., Popel, A.S.: Effect of non axisymmetric hematocrit distribution on non-Newtonian blood flow in small tubes. Biorheology **35**, 69–87 (1998)
30. Pincombe, B., Mazumdar, J., Hamilton-Craig, I.: Effects of multiple stenoses and post-stenotic dilatation on non-Newtonian blood flow in small arteries. Med. Biol. Eng. Comput. **37**(5), 595–599 (1999)
31. Mandal, P.K., Chakravarty, S., Mandal, A., Amin, N.: Effect of body acceleration on unsteady pulsatile flow of non-Newtonian fluid through a stenosed artery. Appl. Math. Comput. **189**(1), 766–779 (2007)
32. Ponalagusamy, R.: Mathematical analysis on effect of non-Newtonian behavior of blood on optimal geometry of microvascular bifurcation system. J. Franklin Inst. **349**(9), 2861–2874 (2012)
33. Ponalagusamy, R.: Pulsatile flow of Herschel–Bulkley fluid in tapered blood vessels. In: Proceedings of the International Conference on Scientific Computing (CSC'13), and World Congress in Computer Science, Computer Engineering, and Applied Computing (WORLDCOMP'13), pp. 67–73 (2013)
34. Merrill, E.W.: Rheology of blood. Physiol. Rev. **49**, 863–888 (1969)
35. Cokelet, G.R., Merrill, E.W., Gilliland, E.R., Shin, H., Britten, A., Wells, E.R.: The rheology of human blood: measurement near and at zero shear rate. Trans. Soc. Rheol. **7**, 303–317 (1963)
36. Dintenfass, L.: Thixotropy of blood and proneness to thrombus formation. Circ. Res. **11**, 233–239 (1962)

37. Owens, R.G.: A new micro structure-based constitutive model for human blood. J. Non-Newton. Fluid Mech. **140**, 57–70 (2006)
38. Blair, G.W.S., Copley, A.L.: An Introduction to Biorheology—Chapter XII on Botanical Aspects by D.C. Spanner. Elsevier, Amsterdam (1974)
39. Priyadharshini, S., Ponalagusamy, R.: Biorheological model on flow of Herschel–Bulkley fluid through a tapered arterial stenosis with dilatation. Appl. Bionics Biomech. **2015**, Article ID 406195 (2015). https://doi.org/10.1155/406195
40. Ponalagusamy, R.: Biological study on Pulsatile flow of Herschel-Bulkley fluid in tapered blood vessels. In: Tran, Q.N., Arabnia, H.R. (eds.) Emerging Trends in Computational Biology, Bioinformatics, and Systems Biology. Chapter 3, vol. 12, pp. 39–50. Kaufmann, San Mateo (2015). https://doi.org/10.1016/B978-0-12-802508-6.00003-X
41. Mandal, P.K.: An unsteady analysis of non-Newtonian blood flow through tapered arteries with a stenosis. Int. J. Non-Linear Mech. **40**(1), 151–164 (2005)
42. Manton, M.J.: Low Reynolds number flow in slowly varying axisymmetric tubes. J. Fluid Mech. **49**, 451–459 (1971)
43. Whitemore, R.L.: Rheology of Circulation. Pergamon, Oxford (1968)
44. Dullaert, K., Mewis, J.: A structural kinetics model for thixotropy. J. Non-Newton. Fluid Mech. **139**, 21–30 (2006)
45. Mujumdar, A., Anthony, N.B., Metzner, A.B.: Transient phenomena in thixotropic systems. J. Non-Newton. Fluid Mech. **102**, 157–178 (2002)
46. Mewis, J., Wagner, N.J.: Colloidal Suspension Rheology. Cambridge University Press, Cambridge (2012)
47. Apostolidis, A.J., Anthony, N.B.: Modelling of the blood rheology in steady-state shear flows. J. Rheol. **58**, 607–633 (2014)
48. Mewis, J.: Thixotropy: a general review. J. Non-Newton. Fluid Mech. **6**, 1–20 (1979)
49. Apostolidis, A.J., Armstrong, M.J., Anthony, N.B.: Modelling of human blood rheology in transient shear flows. J. Rheol. **59**, 275–298 (2015)
50. Yu, M., Wang, S., Fu, J., Peng, Y.: Unsteady analysis for oscillatory flow of magnetorheological fluid dampers based on Bingham plastic and Herschel–Bulkley models. J. Intell. Mater. Syst. Struct. **24**(9), 1067–1078 (2013)
51. Burton, A.C.: Physiology and Biophysics of the Circulation. Medical Publishers, Chicago (1966)

Submit your manuscript to a SpringerOpen journal and benefit from:

- ► Convenient online submission
- ► Rigorous peer review
- ► Open access: articles freely available online
- ► High visibility within the field
- ► Retaining the copyright to your article

Submit your next manuscript at ► springeropen.com